

SHORT-LIVED STAR-FORMING GIANT CLUMPS IN COSMOLOGICAL SIMULATIONS OF $z \approx 2$ DISKS

SHY GENEL^{1,2}, THORSTEN NAAB³, REINHARD GENZEL^{1,4}, NATASCHA M. FÖRSTER SCHREIBER¹, AMIEL STERNBERG², LUDWIG OSER^{3,5}, PETER H. JOHANSSON^{6,7}, ROMEEL DAVÉ⁸, BENJAMIN D. OPPENHEIMER⁹, ANDREAS BURKERT⁵

The Astrophysical Journal, accepted

ABSTRACT

Many observed massive star-forming $z \approx 2$ galaxies are large disks that exhibit irregular morphologies, with ≈ 1 kpc, $\approx 10^{8-10} M_{\odot}$ clumps. We present the largest sample to date of high-resolution cosmological SPH simulations that zoom-in on the formation of individual $M_{*} \approx 10^{10.5} M_{\odot}$ galaxies in $\approx 10^{12} M_{\odot}$ halos at $z \approx 2$. Our code includes strong stellar feedback parameterized as momentum-driven galactic winds. This model reproduces many characteristic features of this observed class of galaxies, such as their clumpy morphologies, smooth and monotonic velocity gradients, high gas fractions ($f_g \approx 50\%$) and high specific star-formation rates ($\gtrsim 1 \text{ Gyr}^{-1}$). In accord with recent models, giant clumps ($M_{\text{clump}} \approx (5 \times 10^8 - 10^9) M_{\odot}$) form in-situ via gravitational instabilities. However, the galactic winds are critical for their subsequent evolution. The giant clumps we obtain are short-lived and are disrupted by wind-driven mass loss. They do not virialise or migrate to the galaxy centers as suggested in recent work neglecting strong winds. By phenomenologically implementing the winds that are observed from high-redshift galaxies and in particular from individual clumps, our simulations reproduce well new observational constraints on clump kinematics and clump ages. In particular, the observation that older clumps appear closer to their galaxy centers is reproduced in our simulations, as a result of inside-out formation of the disks rather than inward clump migration.

Subject headings: galaxies: evolution — galaxies: formation — galaxies: high-redshift — galaxies: structure

1. INTRODUCTION

Star-forming disk galaxies at $z \approx 2$ differ from their local counterparts in several aspects: they are more gas-rich and rapidly star-forming, and have irregular morphologies and high gas velocity dispersions. Spatially resolved observations of their rest-frame UV and optical continuum light often reveal large (≈ 1 kpc) clumps (Elmegreen et al. 2005, 2009; Förster Schreiber et al. 2011b). Clumpy morphologies are also observed with star-formation tracers such as $\text{H}\alpha$ (e.g. the SINS survey; Genzel et al. 2008, 2011). The spectrally resolved line emissions reveal ordered rotation and high velocity dispersions, widespread across the disks at $\approx 50 - 80 \text{ km s}^{-1}$ (Genzel et al. 2006, 2008; Förster Schreiber et al. 2006, 2009; Shapiro et al. 2008; Cresci et al. 2009; Law et al. 2009; Jones et al. 2010; Swinbank et al. 2010).

Theoretically, the large $z \approx 2$ star-forming galaxies have been considered as marginally-unstable thick disks, where the large random motions set the large masses and sizes of unstable regions that collapse into giant clumps (Immeli et al.

2004b; Bournaud et al. 2007, 2008; Genzel et al. 2008; Elmegreen et al. 2008; Agertz et al. 2009; Dekel et al. 2009b; Burkert et al. 2010; Ceverino et al. 2010). In this picture, the high star-formation rates result from the high growth rates of cosmic structures at $z \approx 2$ (Genel et al. 2008), as gas funnels directly from the cosmic web to the vicinity of galaxies in a 'cold-mode' accretion (Kereš et al. 2005; Kereš et al. 2009; Dekel et al. 2009a). However, several observational clues have not yet been addressed in this framework. First, vigorous outflows are observed from a variety of star-forming galaxies at high redshift, both globally (e.g. Pettini et al. 2000; Weiner et al. 2009; Shapiro et al. 2009; Steidel et al. 2010), and from individual giant clumps (Genzel et al. 2011). Second, high signal-to-noise observations of individual giant clumps reveal only minor kinematical signatures, sometimes indicating dynamical masses lower than alternative independent clump mass estimates (Genzel et al. 2011). Third, comparisons of abundance and clustering of galaxies and dark matter halos suggests that at $z \approx 2$, much like at $z = 0$, typically not more than $\approx 10\%$ of the baryons associated with halos of any mass have turned into stars (Moster et al. 2010; Behroozi et al. 2010; Wake et al. 2011), causing some tension with the high efficiency of 'cold-mode' accretion.

Further on, one aspect of the theoretical picture that developed in recent years is that the giant clumps lose angular momentum and energy due to dynamical friction in the disk, clump-clump interactions, and internal torques within the disk, and thereby spiral in to the center of the galaxy. This has been based on two main lines of argument. First, age gradients have been inferred in clumpy disks from the presence of a redder/older component often coinciding or close to the galaxy center (van den Bergh et al. 1996; Elmegreen et al. 2009). Also, a correlation has been found between the relative dynamical dominance of that central component to a (metallicity-based) age estimate for the system, which has been interpreted as indicative of a time sequence, where older

¹ Max Planck Institut für extraterrestrische Physik, Giessenbachstrasse, 85748 Garching, Germany; shy@mpe.mpg.de; genzel@mpe.mpg.de; forster@mpe.mpg.de

² Sackler School of Physics and Astronomy, Tel Aviv University, Tel Aviv 69978, Israel; amiel@wise.tau.ac.il

³ Max Planck Institut für Astrophysik, Karl-Schwarzschild-Str. 1, 85741 Garching, Germany; naab@mpa-garching.mpg.de; oser@usm.lmu.de

⁴ Department of Physics, Le Conte Hall, University of California, Berkeley, CA 94720

⁵ Universitäts-Sternwarte München, Scheinerstr. 1, D-81679 München, Germany; burkert@usm.lmu.de

⁶ Department of Physics, University of Helsinki, Gustaf Hällströmin katu 2a, FI-00014 Helsinki, Finland

⁷ Finnish Centre for Astronomy with ESO, University of Turku, Väisäläntie 20, FI-21500 Piikkiö, Finland; phjohans@astro.helsinki.fi

⁸ Astronomy department, University of Arizona, Tuscon, AZ 85721; rad@as.arizona.edu

⁹ Leiden Observatory, Leiden University, PO Box 9513, 2300 RA Leiden, the Netherlands; oppenheimer@strw.leidenuniv.nl

systems have had more time to transform part of their disks into bulges via clump migration (Genzel et al. 2008). Second, numerical simulations, both of isolated unstable disks (Immeli et al. 2004a; Bournaud et al. 2007; Elmegreen et al. 2008; Bournaud et al. 2009) and of cosmological $z \approx 2$ disks (Agertz et al. 2009; Ceverino et al. 2010), find the clumps to evolve in that fashion, and theoretical considerations also suggest there should be a significant inflow rate inside the disk (Dekel et al. 2009b; Bournaud et al. 2011). Recently Förster Schreiber et al. (2011b) used deep higher-resolution NIC2 imaging to identify more robustly clumps in rest-frame optical emission, and, in combination with AO-assisted SINFONI $H\alpha$ observations and ACS imaging, radial trends in clump stellar age with distance to galaxy center were inferred. This result appears consistent with the theoretical inspiraling picture, as noted by Ceverino et al. (2011).

Therefore, a crucial issue is whether giant clumps can survive long enough to become stellar-dominated and/or sink to the centers of their galaxies, contributing to the buildup of bulges. Conflicting theoretical claims have been made (Murray et al. 2010; Krumholz & Dekel 2010), while probing that question directly with observations is a difficult task. Therefore, the qualitative agreement between simulations and observations has been interpreted as supporting the picture of long-lived migrating clumps. However, none of the cosmological or isolated simulations reported so far (but see Sales et al. 2010), which find long-lived migrating clumps, include strong galactic winds, which as noted already are directly observed. As the ‘clumpy phase’ appears to be ubiquitous at $z \approx 1-3$, it is of fundamental importance for our understanding of galaxy formation to know what role giant clumps play in building bulges/spheroids.

In this paper, we demonstrate as a proof of principle that incorporating galactic superwinds resulting from stellar feedback into the existing theoretical picture, can have important implications for our understanding of $z \approx 2$ disks and their evolution. We use hydrodynamical cosmological simulations to investigate the formation and properties of a sample of star-forming disks. We use a phenomenological model for the generation of galactic winds to test a scenario in which galactic superwinds are a major driving force in shaping galaxy disks at high redshift. The phenomenological a priori parameters of our model match the observed properties of winds in the type of galaxies we are considering. Our results are heavily dependent on this phenomenology, hence the uncertainty in the observations of such winds is a source of uncertainty for the basic assumptions of our model. However, we find that the implications of implementing such winds in simulations, namely that the giant clumps are short-lived transient features, and thus do not survive to migrate to the centers of their galaxies to form a bulge, are consistent with the existing observational constraints. Hence, we propose a new scenario for the evolution of $z \approx 2$ clumpy disks.

2. THE SIMULATIONS: CODE AND SETUP

We run ‘zoom-in’ cosmological simulations focused on individual halos taken from the $72h^{-1}$ Mpc cosmological dark matter simulation presented in Oser et al. (2010) for the following cosmological parameters: $\Omega_m = 0.26$, $\Omega_\Lambda = 0.74$, $\Omega_b = 0.044$, $h = 0.72$, $n = 0.95$ and $\sigma_8 = 0.77$. As we focus on massive disks with high star-formation rates (SFR), we select at $z = 2$ halos of $\approx 10^{12} M_\odot$ with instantaneous dark matter growth rates exceeding $500 M_\odot \text{ yr}^{-1}$ and that had no major merger (mass ratio $< 3 : 1$) since $z = 3$ (see Genel et al.

2008). The second criterion selects approximately half of the halos of that mass at that redshift, and together these criteria are met by $\approx 15\%$ of those halos, i.e. our galaxies form in halos that are neither the most ‘typical’ nor very ‘special’ or rare. From this sample, we randomly selected nine halos and generated ‘zoom-in’ initial conditions for re-simulations including baryons, as in Oser et al. 2010, 2011. Our scheme results in high-resolution regions of ≈ 5 Mpc comoving, on a side, i.e. approximately 1000 times larger (in volume) than our main halos at $z \approx 2$. The mass resolution of our simulations is $8 \times 10^5 M_\odot$ and $5 \times 10^6 M_\odot$ for baryonic and high-resolution dark matter particles, respectively. The gravitational softening lengths of baryonic particles are $200h^{-1}$ pc, constant in comoving units, resulting in physical softening lengths of ≈ 90 pc at $z = 2$.

The cosmological box is evolved to $z = 2$ using a version of the N-body/SPH code *Gadget-2* (Springel 2005) that is very similar to the one described in Oppenheimer & Davé (2006, 2008). This version includes ionisation and heating by a uniform background radiation (Haardt & Madau 2001) in the optically thin limit, atomic cooling down to $T = 10^4 \text{ K}$ from hydrogen and metals, star-formation and feedback, as well as mass loss and metal enrichment from AGB stars and supernovae of types II and Ia.

The Oppenheimer & Davé (2008) version of the code uses the Springel & Hernquist (2003) star-formation prescription, where stars form stochastically from the gas according to a Schmidt (1959) law that reproduces the Kennicutt (1998) gas surface density to star-formation relation. In addition, that prescription includes a sub-grid model for supernova feedback that results in an effective equation of state for the star-forming gas $P \propto \rho^{\gamma(\rho)}$, where P is the gas pressure, and ρ its physical density. The running index $\gamma(\rho)$ in the Springel & Hernquist (2003) model is rather high at low and medium densities (a stiff equation of state), but becomes negative at high densities, such that the thermal Jeans mass M_J can rapidly drop below the resolution of the simulation (Hopkins & Quataert 2010). The stiffness of this equation of state at medium densities allows construction of stable disk models (e.g. Springel et al. 2005). It is less relevant for simulations of marginally-unstable disks. Therefore, we replaced the star-formation model in the Oppenheimer & Davé (2008) code with the Schaye & Dalla Vecchia (2008) approach. There, the usual cooling and heating operate at $\rho < \rho_{EOS}$, while for $\rho > \rho_{EOS}$ a polytropic equation of state with $\gamma = 4/3$ is implemented. This ensures that the (thermal) Jeans mass M_J remains constant with varying density and does not become unresolved. Here $\rho_{EOS} = 0.1 \text{ cm}^{-3}$ is defined such that $M_J \approx 1.4 \times 10^7 M_\odot$ at $\rho = \rho_{EOS}$ and $T = 10^4 \text{ K}$. Star-formation is parameterised as

$$\frac{d\rho_*}{dt} = \frac{\rho}{1 \text{ Gyr}} \left(\frac{\rho}{\rho_{th}} \right)^{0.26}, \quad (1)$$

with the star-formation density threshold $\rho_{th} = \rho_{EOS} = 0.1 \text{ cm}^{-3}$. This reproduces the Kennicutt (1998) star-formation relation (Schaye & Dalla Vecchia 2008). A further addition we introduced to the code is that we calculate the local minimum (over all directions) of the gas surface density $\rho^2/|\nabla\rho|$ (Gnedin et al. 2009), and suppress star-formation if $\rho^2/|\nabla\rho| < 10^{21} \text{ cm}^{-2}$. This modification has only minor consequences for our results.

The feedback scheme developed by Oppenheimer & Davé (2006, 2008) builds on the kinetic feedback scheme of Springel & Hernquist (2003), where star-forming gas parti-

cles are stochastically kicked with velocities in the $\mathbf{v} \times \mathbf{a}$ direction, where \mathbf{v} is the particle's velocity prior to the kick and \mathbf{a} its acceleration. Oppenheimer & Davé (2006, 2008) introduced a significant modification to this mechanism by tuning the two parameters that control the wind. In their prescription, the magnitude of the kick is $v_{wind} = \sigma(2 + 3\sqrt{f_L - 1})$ and the mass-loading factor

$$\frac{\dot{M}_W}{SFR} \equiv \eta = \frac{\sigma_0}{\sigma}, \quad (2)$$

where $f_L \approx 1 - 2$ is the luminosity factor, σ is the 'velocity dispersion' of the galaxy that is calculated from its mass¹⁰, and σ_0 is a constant (here $\sigma_0 = 300 \text{ km s}^{-1}$, as in Oppenheimer & Davé (2006)). Introducing σ -dependencies, these two parameters then scale with the mass of the galaxy, following the theory of momentum-driven winds induced by the radiation pressure from young stars (Murray et al. 2005; Zhang & Thompson 2010).

The momentum budget available from feedback from young stars is somewhat uncertain. Murray et al. (2005) estimate the momentum injection from radiation pressure of OB stars (per unit stellar mass formed) to be $\approx 200 \text{ km s}^{-1}$, and a similar amount of momentum from supernova explosions. Ostriker & Shetty (2011), however, estimate the specific momentum available from supernovae to be $\approx 3000 \text{ km s}^{-1}$. In addition, high dust column densities can provide large optical depths that increase the amount of momentum injection by radiation pressure by factors of several (e.g. Murray et al. 2010). Finally, stellar winds can also inject similar amounts of momentum (Leitherer et al. 1999). We use $v_{wind} = \sigma(4 + 4.29\sqrt{f_L - 1})$, such that the value that we use for the momentum injection per unit stellar mass formed, $\eta v_{wind} \lesssim 2500 \text{ km s}^{-1}$, is a physically plausible value, even if on the high side. Note that we use higher wind velocities than in Oppenheimer & Davé (2008). This ensures the escape of all wind particles from the disk, in particular from regions in the disk that have higher escape velocities than the mean one. This change is necessary, since we have a significantly higher resolution in this work, such that the center of the galaxy may become dense enough for its escape velocity to be higher than that at the edge of the disk.

The scalings of the momentum-driven winds are in accordance with observational evidence for the scalings of galactic winds (e.g. Martin 2005; Rupke et al. 2005). The typical velocities we obtain with this model for the central galaxies considered are $\approx 400 - 700 \text{ km s}^{-1}$, in agreement with observations. The typical mass-loading factor for our central galaxies is $\eta \approx 4$, also in order-of-magnitude agreement with observations, although the observational determination of the mass-loading factors is far less certain than that of the wind velocities (e.g. Erb et al. 2006; Genzel et al. 2011 and references therein).

In the Springel & Hernquist (2003) and Oppenheimer & Davé (2008) models, subsequent to being given a velocity kick, gas particles are temporarily decoupled from hydrodynamic interactions to allow them to propagate out of their star-formation sites and eventually

leave their galaxies. When simply giving gas particles momentum kicks rather than using a more sophisticated physical model (in a better-resolved interstellar medium), the only way to achieve winds that escape the vicinity of the galaxies (rather than efficiently becoming a galactic fountain) is by using the temporary decoupling method (Dalla Vecchia & Schaye 2008). Moreover, even high resolution simulations of isolated galaxies have so far had difficulties in forming efficient winds when having full hydrodynamics and cooling (e.g. Mac Low & Ferrara 1999; Fujita et al. 2004; Dubois & Teyssier 2008). However, such winds are observed, and emerge out of $z \approx 2$ galaxies to large distances (Steidel et al. 2010). Therefore, we keep the decoupling prescriptions adopted by Oppenheimer & Davé (2008). We have, however, modified the Oppenheimer & Davé (2008) code to ensure that the velocity kicks are perpendicular to the disk (e.g. Bordoloi et al. 2011, Bouché et al. in prep.). This is done by calculating the direction of the velocity kicks wind particles are given as $(\mathbf{v} - \mathbf{v}_{gal}) \times (\mathbf{a} - \mathbf{a}_{gal})$, where \mathbf{v} , \mathbf{a} are the velocity and acceleration of the launched wind particle just before the kick, and \mathbf{v}_{gal} , \mathbf{a}_{gal} are the velocity and acceleration of the center-of-mass of the galaxy, i.e. $\mathbf{v} \times \mathbf{a}$ is calculated in the inertial frame of the galaxy.

The theoretical considerations and actual observations of winds from galaxies are augmented by further motivation for using the Oppenheimer & Davé (2008) model, namely this strong galactic winds model successfully matches several important observations:

- Properties of the intergalactic medium, such as metallicity and ionization state (Oppenheimer & Davé 2006, 2009; Davé et al. 2010).
- The galaxy mass-metallicity relation (Finlator & Davé 2008; Davé et al. 2011a).
- High galactic gas fractions at high redshift (Section 3.1 and Davé et al. 2011a).
- Low fraction of cosmic baryons in galaxies at all redshifts (Section 3.1 and Davé et al. 2011b).

It should be kept in mind, however, that the simulations presented in this work have much higher resolution than previous works that employed the Oppenheimer & Davé (2008) model. Therefore, some adverse side effects cannot be excluded before a large cosmological box is run with a similarly high resolution. Indeed, we corrected for one such side effect by using increased velocities (see above).

3. RESULTS

3.1. Global properties

We begin by considering several global properties of the galaxies formed in our sample of nine 'zoom-in' simulations and comparing them with observational constraints. Table 1 gives halo masses, peak circular velocities, sizes, gas and stellar masses, gas fractions and SFRs for the main galaxies in our sample. This sample can be compared to a 'median disk' from the SINS survey, whose properties are given in Table 1 as well. Bearing in mind the uncertainties in the observational quantities, which are of roughly a factor of two for the masses and SFRs, and the unavoidable differences in the definitions of some of the quantities between simulations and observations (see footnotes to Table 1), it seems that our simulated galaxy sample is overall a good match to the disks observed

¹⁰ Galaxy dynamical masses are calculated based on an on-the-fly group finder, and then used to calculate $\sigma \equiv 200[(M_{dyn}/5 \cdot 10^{12} M_\odot)h(H(z)/H_0)]^{1/3}$. For calculation efficiency, a friends-of-friends (FOF) algorithm is used. We use a linking length $b = 0.025(\frac{H(z)}{H(0)})^{1/3}$ that is an improvement over the constant b used in Oppenheimer & Davé (2008), since it is calibrated to the SKID group finder at various redshifts.

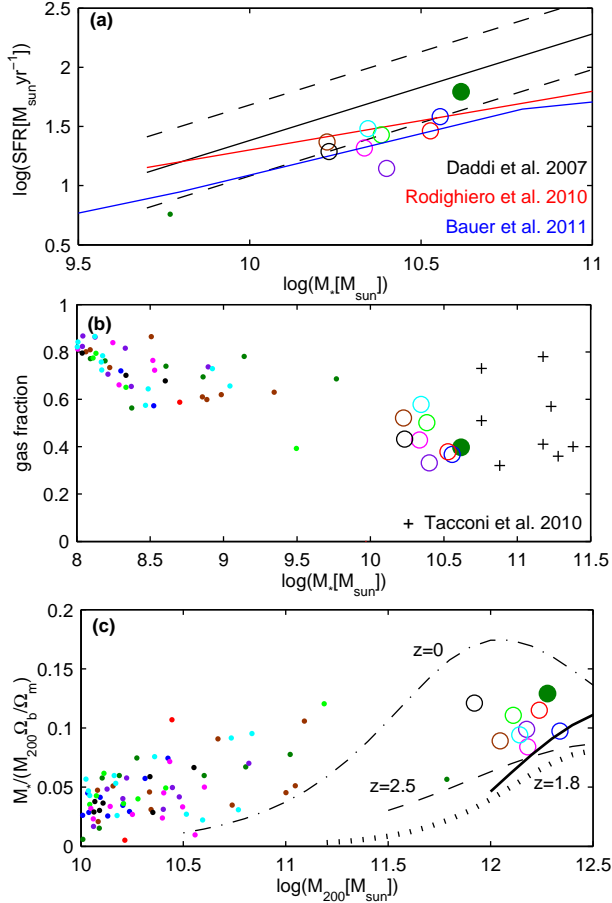


FIG. 1.— Global properties of nine ‘zoom-in’ simulations at $z=2$, where each color represents one simulation, with its main galaxy (circles) and the smaller galaxies that formed in neighbouring dark matter halos inside the zoomed-in region (dots). Only galaxies that are central in their own halos are shown, i.e. leaving out satellite galaxies that are already inside the main zoomed-in halo. In all panels *s224* is marked with a filled circle. *Top*: SFR versus stellar mass. The observed Daddi et al. (2007) relation for $z=2$ (solid; standard deviation is dashed), Rodighiero et al. (2010) relation for $1.5 < z < 2$ (red) and Bauer et al. (2011) relation for $1.5 < z < 3$ (blue), all corrected for a Chabrier (2003) initial mass function, are plotted on top of the simulation results, and demonstrate a reasonable match between our simulated galaxies and observations. *Middle*: Gas fractions (gas mass over baryonic mass) versus stellar mass. There is a trend of increasing gas fractions with decreasing mass, and the fractions for our main sample are $\approx 40\%$, in good agreement with observations at $z \approx 2.2$ (Tacconi et al. 2010, *pluses*). *Bottom*: ‘Baryon conversion efficiency’ as a function of halo mass. The highest efficiencies of $\approx 10\%$ are obtained at $M_{\text{halo}} \gtrsim 10^{12} M_{\odot}$, in rough agreement with results obtained from matching observations to dark matter halo models, which are taken from Moster et al. (2010) for $z=2.5$ (dashed), $z=1.8$ (dotted) and $z=0$ (dashed-dotted), as well as from Wake et al. (2011) for $1 < z < 2$ (solid). In all panels, the baryonic quantities (i.e. all but M_{200}) are computed inside $3R_{1/2}$, where $R_{1/2}$ is the stellar half-mass radius within $0.2R_{200}$.

in the SINS survey. Nevertheless, our simulated sample may be somewhat ‘scaled-down’ compared to the observed sample, by a factor of approximately two in the masses and SFRs, and less than that in size.

In Figure 1, panel (a) shows the SFR versus stellar mass (M_*) plane for central galaxies in the high-resolution region of each of our simulations. The simulated galaxies populate the same region as observed $z \approx 2$ galaxies, taken from Daddi et al. (2007) (black), Bauer et al. (2011) (blue) and Rodighiero et al. (2010) (red). The scatter around the mean Daddi et al. (2007) relation is roughly 0.5dex (dashed), and

the uncertainty in those measurements is of similar magnitude, as evident from the differences between the three lines. The SFR history in the central galaxies is rather constant, as demonstrated in Table 1 by comparing the current SFR to its past average. Figure 1(b) presents gas fractions ($f_g \equiv \frac{M_g}{M_g + M_*}$) versus stellar mass. There is a trend of increasing gas fractions with decreasing mass (see also Davé et al. 2011a), and the fractions for our main sample are $\approx 40\%$, in good agreement with observations at $z \approx 2.2$ (Tacconi et al. 2010, *pluses*). Figure 1(c) shows ‘baryon conversion efficiencies’ ($\frac{M_*}{M_{200}\Omega_b/\Omega_m}$) versus halo mass. Our simulated halos are presented (symbols) alongside the same quantity as it is estimated from comparisons of galaxy and halo clustering and abundances (Moster et al. 2010; Wake et al. 2011; curves). The baryon conversion efficiency is a strong function of mass in our simulations, though not as strong as observations indicate, such that small dark matter halos in our simulations probably host too massive galaxies (see also Davé et al. 2011b).

These observed correlations are important constraints that should be reproduced in realistic simulated galaxies. The SFR versus stellar mass ‘main sequence’ relation has received significant attention in recent years and it is a key constraint for galaxy evolution. The gas fraction of galaxies is a dominant factor in their dynamics, and the baryonic conversion efficiency controls the number density of galaxies. Regardless of the imperfect agreement with observations (in particular at halo/galaxy masses below the scale that is the focus of this paper), the global correlations in Figure 1 are a result of the galactic winds model we are using, without which they would compare much worse to the observations (Davé 2008, 2009; Davé et al. 2011a,b). For example, the three clumpy disks simulated by Ceverino et al. (2010) in a cosmological context with less effective feedback have gas fractions as low as 18%, 14%, 4% and baryon conversion efficiencies as high as 0.26, 0.22, 1.14, both indicating too little suppression of star formation when compared to observations.

It is apparent that our prescriptions dump more momentum per baryon than used in, e.g., Ceverino et al. (2010), Bournaud et al. (2007) and Agertz et al. (2009). As such, our sub-grid models may seem extreme and the negative impact of winds on the clump survival (Section 3.3) overdone. However, consider what would happen if we switch off this recipe, or substantially turn down its efficacy. To this end, we have performed additional experiments, where we used less efficient winds, either by injecting less momentum (using slower winds, or winds with lower mass-loading factors), or by not temporarily decoupling the wind particles from the hydrodynamics. If the winds are not decoupled they cannot escape the vicinity of the galaxies and are ineffective (Dalla Vecchia & Schaye 2008). In these experiments, we obtained galaxies with very different properties, in agreement with similar results from the literature (reviewed above), and in contrast with observations. For example, when halo *s224* is simulated when winds are not temporarily decoupled from the hydrodynamics, we obtain a central galaxy at $z=2$ with low specific star formation rate (0.6 Gyr^{-1} compared to 1.5 Gyr^{-1} in the fiducial model), low gas fraction (8.6% compared to the fiducial 40%), high baryonic conversion efficiency (0.26 compared to the fiducial 0.129), high (and peaked) rotation curve (with the peak at 555 km s^{-1} compared to the fiducial 278 km s^{-1}), and small size ($R_{1/2} = 1 \text{ kpc}$ compared to $R_{1/2} = 3.3 \text{ kpc}$). Moreover, the clumpy nature of

the galaxies, discussed in detail in the following sections, is also lost under such conditions.

3.2. Disk and clump properties

In Figure 2 we present gas surface density maps of four galaxies from our sample (large panels). The mean gas surface densities inside radii of $\approx 4-8$ kpc have values ranging from $\approx 50-300 M_\odot \text{pc}^{-2}$. However, the gas surface density is far from constant in the disk, but rather exhibits strong local maxima, to which we hereafter refer as 'clumps'. The perturbed morphologies, and the clumps, are the result of disk instabilities rather than external interactions, as will be discussed in Section 3.3. The typical gas surface densities of clumps are up to ten times higher than the mean disk surface densities, i.e. $\approx 500-3000 M_\odot \text{pc}^{-2}$. The clumps tend to be embedded inside transient ring-like features, although not exclusively. The clumpy morphologies of the gas (and hence SFR) are clearly visible also after being smoothed to the resolution of typical good AO-assisted observations (FWHM=1.5 kpc), as shown in the small panels, in face-on as well as edge-on views (top and bottom small panels for each galaxy). After this smoothing, the typical contrast ratio (clump-to-disk mean surface densities) is reduced to ≈ 3 . The total SFR in all clumps is $\lesssim 20\%$ of the total disk SFR. These properties match those of observed $z \approx 2$ clumpy disks very well (Genzel et al. 2011; Förster Schreiber et al. 2011a).

We now discuss one galaxy from our sample, *s224*, in greater detail, as a representative case. The gas is distributed mainly in a ring with a radius of ≈ 3 kpc (Figure 3(c)). The ring, which is transient, formed from spiral features in the disk rather than by an interaction (there are no interactions with stellar mass ratios $< 20 : 1$ since $z \approx 3$). Several clumps are embedded in the ring, and appear as SFR overdensities (Figures 3(a) and 3(d)). The gas vertical velocity dispersion σ_z is $\approx 20-100 \text{ km s}^{-1}$ (Figure 3(b)), in agreement with observed values at $z \approx 2$. The high density regions and clumps are minima of σ_z , as denser gas dissipates the random motions more quickly and is less prone to stirring effects such as external accretion (Aumer et al. 2010). The disk shows regular rotation (Figure 3(e)), indicative of its quiet merger history (Shapiro et al. 2008).

Hereafter, for *s224* we use a threshold of face-on gas surface density $\Sigma_g > 1000 M_\odot \text{pc}^{-2}$ to define clumps. With this definition, we identify four clumps (Figure 3(a)). We calculate their sizes, masses, gas fractions and SFRs inside the region where $\Sigma_g > 1000 M_\odot \text{pc}^{-2}$, and list them in Table 1. The clumps have masses of $\approx (5 \times 10^8 - 10^9) M_\odot$,¹¹ and they are very gas rich ($f_g \sim 60\%$). The clumps themselves have low ($\approx 50 \text{ km s}^{-1} \text{ kpc}^{-1}$) velocity gradients, not much larger than the galaxy-wide average velocity gradient, which is typically $\approx 30 \text{ km s}^{-1} \text{ kpc}^{-1}$ at a few kiloparsecs from the center.

¹¹ Observed clump masses from the literature tend to be larger, and several clumps with even $\approx 10^{10} M_\odot$ are known. Several biases can contribute to this apparent discrepancy. First, our simulated disks are less massive than most of the host galaxies of the most massive observed clumps. Therefore, it is the clump-to-disk mass ratio that should be compared. Second, some of the most massive observed clumps have atypical clump-to-disk mass ratios, some of which may be special cases such as clump mergers or galaxy minor mergers. Third, there is no standard for identifying clumps and setting their borders. Such differences may introduce poorly controlled systematics between different studies. The typical clump-to-disk mass ratio reported in Elmegreen & Elmegreen (2005) is 1%, and in Förster Schreiber et al. (2011b) it is roughly 2%. This is, at face value, 2–3 times higher than the clump-to-disk mass ratios found in our simulations.

3.3. Clump formation and disruption

Defining a Q parameter for disk instability (Toomre 1964) of

$$Q \equiv \frac{\kappa \sqrt{\sigma_g^2 + c_s^2}}{\pi G \Sigma_g} \quad (3)$$

where σ_g is the local gas velocity dispersion, c_s the gas sound speed, and

$$\kappa = \sqrt{3} \sqrt{\frac{GM_{\text{tot}}(< R)}{R}} / R \quad (4)$$

(e.g. Dekel et al. 2009b), we find that the clumps are local minima with $Q \ll 1$ (Figure 3(f)). The clumps form in-situ: they are not accreted from outside the disk, but rather form inside the disk via gravitational instability in an environment that has $Q \approx 1$. This is consistent with the theoretical framework that is described in the Introduction, and in particular in agreement with other cosmological simulations (Agertz et al. 2009; Ceverino et al. 2010, 2011). The clump masses are 1–2 orders of magnitude larger than the thermal Jeans mass, but match the 'largest unstable Jeans scale' (the 'Toomre mass') in a turbulent disk

$$M_{J,\sigma} \approx \left(\frac{\sigma_g}{v_{\text{rot}}}\right)^2 M_{\text{disk}} \gtrsim \left(\frac{20}{250}\right)^2 \times 6 \times 10^{10} M_\odot \approx 4 \times 10^8 M_\odot \quad (5)$$

(Genzel et al. 2008; Dekel et al. 2009b), which is driven to high values by the large random motions in the disk.

A notable characteristic of the clumps is their short lifetimes, ≈ 50 Myr, or about half a disk orbital time. The top row in Figure 4 demonstrates the disruption of a clump in *s224* by showing a time series of gas surface density maps. In the upper right-most panel of Figure 4, the gas masses of three clumps are shown as a function of time (*solid*), demonstrating their rapid formation and disruption. In contrast, the bottom row of Figure 4 shows the evolution of the same clump in an experiment where we temporarily turn the wind off. The clump does not disrupt, instead it collapses further and virialises, and subsequently migrates to the galaxy center. This demonstrates that the clumps are destroyed by the wind feedback, and do survive (our equation-of-state is sufficiently soft to allow for this), as found in previous simulations, when such feedback is absent (or much weaker than adopted in our sub-grid model).

The reason for the disruption of clumps by the wind is the following. In our model, the wind mass-loading factor (i.e. the outflow rate over the SFR) for $10^{10.5} M_\odot$ galaxies at $z = 2$ is $\eta \approx 4$ (Oppenheimer & Davé 2008), and the velocity ranges between $\approx 400-700 \text{ km s}^{-1}$. These wind parameters agree well with recent observational detections of gas outflowing from $z \approx 2$ galaxies (Steidel et al. 2010) and clumps (Genzel et al. 2011). Star-formation in the clumps proceeds on a timescale $T_{\text{SF}} \approx 300$ Myr (according to the Kennicutt (1998) relation), thus winds drive gas out of the clumps on a timescale $\approx T_{\text{SF}}/\eta \approx 100$ Myr, which is comparable to the disk orbital time. The consequence is that the gas surface density in the clumps decreases faster than the rate at which it is replenished by the instability inside the disk, and so clump regions move from $Q \lesssim 1$ to $Q \gtrsim 1$ (and thus stop collapsing) within a time that is shorter than the disk orbital time. The short lifetimes we find are consistent with the upper limits of $\approx 300-500$ Myr derived for the stellar populations

TABLE 1
GALAXY AND CLUMP PROPERTIES

	halo mass	baryon conversion	peak	Half-mass	Stellar mass	Gas mass	Gas fraction	SFR ^(b)	Number of	$\frac{\text{SFR}}{\langle \text{SFR} \rangle}$ ^(d)
	M_{200}	efficiency	$V_c \equiv \sqrt{GM/R}$	radius $R_{1/2}$ ^(a)	M_* ^(b)	M_g ^(b)	f_g ^(b)	$[\text{M}_\odot \text{yr}^{-1}]$	clumps ^(c)	
	$[10^{12} \text{M}_\odot]$	$\frac{M_*}{M_{200} \Omega_b / \Omega_m}$	$[\text{kms}^{-1}]$	$[\text{kpc}]$	$[10^{10} \text{M}_\odot]$	$[10^{10} \text{M}_\odot]$				
<i>median SINS disk</i> ^(e)	-	-	237	4.6	4.4	1.9 ^(f)	30% ^(f)	65	5.5	-
<i>median simulated disk</i>	1.5	0.099	238	3.5	2.4	2.1	43%	27	5	1.31
<i>s224</i>	1.90	0.129	278	3.3	4.1	2.7	40%	62	5	1.45
<i>s263</i>	2.18	0.097	289	3.5	3.6	2.1	37%	38	3	1.51
<i>s361</i>	1.29	0.111	238	4.6	2.4	2.4	50%	27	0	0.75
<i>s377</i>	1.52	0.084	252	3.3	2.2	1.6	43%	21	6	1.00
<i>s383</i>	1.73	0.115	253	3.2	3.4	2.1	38%	29	6	0.86
<i>s396</i>	1.50	0.099	225	3.8	2.5	1.2	33%	14	5	0.65
<i>s447</i>	1.11	0.089	229	3.5	1.7	1.8	52%	23	4	1.60
<i>s466</i>	1.39	0.094	238	5.7	2.2	3.0	58%	30	7	1.41
<i>s809</i>	0.83	0.121	207	2.6	1.7	1.3	43%	19	5	1.31
<i>clump-1</i>	-	-	-	0.45	0.022	0.044	67%	2.7	-	-
<i>clump-2</i>	-	-	-	0.27	0.02	0.04	67%	2.3	-	-
<i>clump-3</i>	-	-	-	0.22	0.022	0.025	53%	1.5	-	-
<i>clump-4</i>	-	-	-	0.42	0.027	0.07	72%	3.7	-	-

NOTE. — (a) For galaxies: stellar (3D) half-mass radius within $0.2R_{200}$, for clumps: gas half-mass radius inside the region with $\Sigma_g > 1000 \text{M}_\odot \text{pc}^{-2}$; (b) For galaxies: inside $3R_{1/2}$, for clumps: inside the region with $\Sigma_g > 1000 \text{M}_\odot \text{pc}^{-2}$; (c) Identified as local overdensities in the gas surface density, excluding the galaxy center; (d) $\langle \text{SFR} \rangle$ is the mean SFR between $z = 3$ and $z = 2$; (e) Calculated using the nine galaxies from Förster Schreiber et al. (2009) that are defined as ‘disks’ and have kinematic modeling. Differences to the definitions adopted for the simulations are: V_c is the observed maximum rotation velocity of the H α -emitting gas; $R_{1/2}$ is calculated from projected H α light; all quantities are galaxy-integrated values; the clumps for MD41, BX389 and BX610 are overdensities of rest-frame optical light. Stellar masses and SFRs are estimated with SED modeling, and gas masses are estimated from the SFRs by using the empirical Bouché et al. (2007) star-formation relation. Data are taken from Genel et al. (2008); Cresci et al. (2009); Förster Schreiber et al. (2009, 2011a), and are all scaled for a Chabrier (2003) initial mass function; (f) The gas masses are probably lower bounds, since we use the steep Bouché et al. (2007) star-formation relation to derive them, as in Förster Schreiber et al. (2009). If the Kennicutt (1998) or Genel et al. (2010) relations were used, the gas masses would increase by up to a factor ≈ 3 . That would increase the gas fractions to $\approx 50\% - 60\%$. Indeed, the direct CO observations in Tacconi et al. (2010) and Daddi et al. (2010) indicate $\approx 45 - 65\%$ as the most favourable values.

in the clumps (Elmegreen et al. 2009; Förster Schreiber et al. 2011a). This is because the mean stellar ages of the clumps in our simulations are larger than the lifetimes of the clumps as star-forming overdensities (see Figure 5 and accompanying discussion below).

Given the masses and sizes of clumps (Table 1), their circular velocities equal $\sqrt{GM/R} \approx 80 - 100 \text{kms}^{-1}$. This is significantly larger than the velocity dispersion of the gas within them or their rotational velocities (in particular if the galaxy-wide average velocity gradient is subtracted as ‘background’). Typically the clumps have $v_{\text{rot}}^2 + 2\sigma_g^2 \approx 0.6(GM/R)$, or $|\frac{U}{K}| \gtrsim 3$, where U is their gravitational potential energy and K the internal kinetic energy. Thus, they are neither supported by pressure nor by rotation, and in fact they are not virialised. This is due to continuous feedback on a timescale shorter than the dynamical time, preventing virialisation before disruption.

The clumps consist two types of stellar populations. First, ‘background stars’, which are part of the stellar disk at the locations where clumps form but are not necessarily bound to them, with an age distribution similar to that of the stellar disk as a whole. A dynamically cold stellar component also takes part in the instability, in addition to the gas, such that the local density of old ‘background stars’ is increased in some clumps compared to the clump surroundings. The ‘background stars’ comprise most of the stellar mass of the clumps, as the clumps typically convert just about 10% of their peak gas mass into stars throughout their lifetime. Second are ‘clump stars’, which form over the lifetime of a clump, and are almost all bound to their clumps, constituting typically up to $\approx 20\%$ of their stellar masses.

As a result, the mean age of the stellar populations inside clumps follows the global spatial age distribution of the ‘back-

ground stars’ of the disk, with an additional small contribution of the ‘clump stars’, which makes the clumps typically be local age minima. We find that the stellar disks in our simulations have a negative age (and metallicity) gradient, which will be discussed in detail in future work. Therefore, the mean ages of clumps also present a spatial gradient, such that clumps with older stellar populations are closer to the galaxy center. This is shown in Figure 5. The trend we find is qualitatively consistent with observations, in spite of the fact that no individual clump actually migrates to the galaxy center as its stellar populations become older. A quantitative comparison to observations cannot be performed yet, as measuring clump ages requires high-resolution, deep data taken with various instruments. For example, Förster Schreiber et al. (2011b) was able to measure clump ages for only one $z \approx 2$ galaxy from their sample, BX482, which are shown in Figure 5 (*squares*). These measurements rely on H α equivalent width, and they are very sensitive to the assumptions made regarding the star-formation history. Therefore, they should be taken only as relative ages, not absolute ones (Förster Schreiber et al. 2011b). A linear fit in the log-log plane to the clump age-distance relation from our simulations yields a slope of -0.57 ± 0.14 . The corresponding slope for the BX482 points shown in Figure 5 is -2.06 ± 0.63 . Future comparisons of this correlation with larger galaxy samples, and with an improved treatment of possible biases both on the theoretical and observational sides, may be able to distinguish the slope we find from the -1.05 slope found by Ceverino et al. (2011) for the case of migrating clumps. To conclude, the mere existence of an age gradient should not necessarily be interpreted as supporting the clump migration scenario (see also Förster Schreiber et al. (2011b) for additional alternative interpretations).

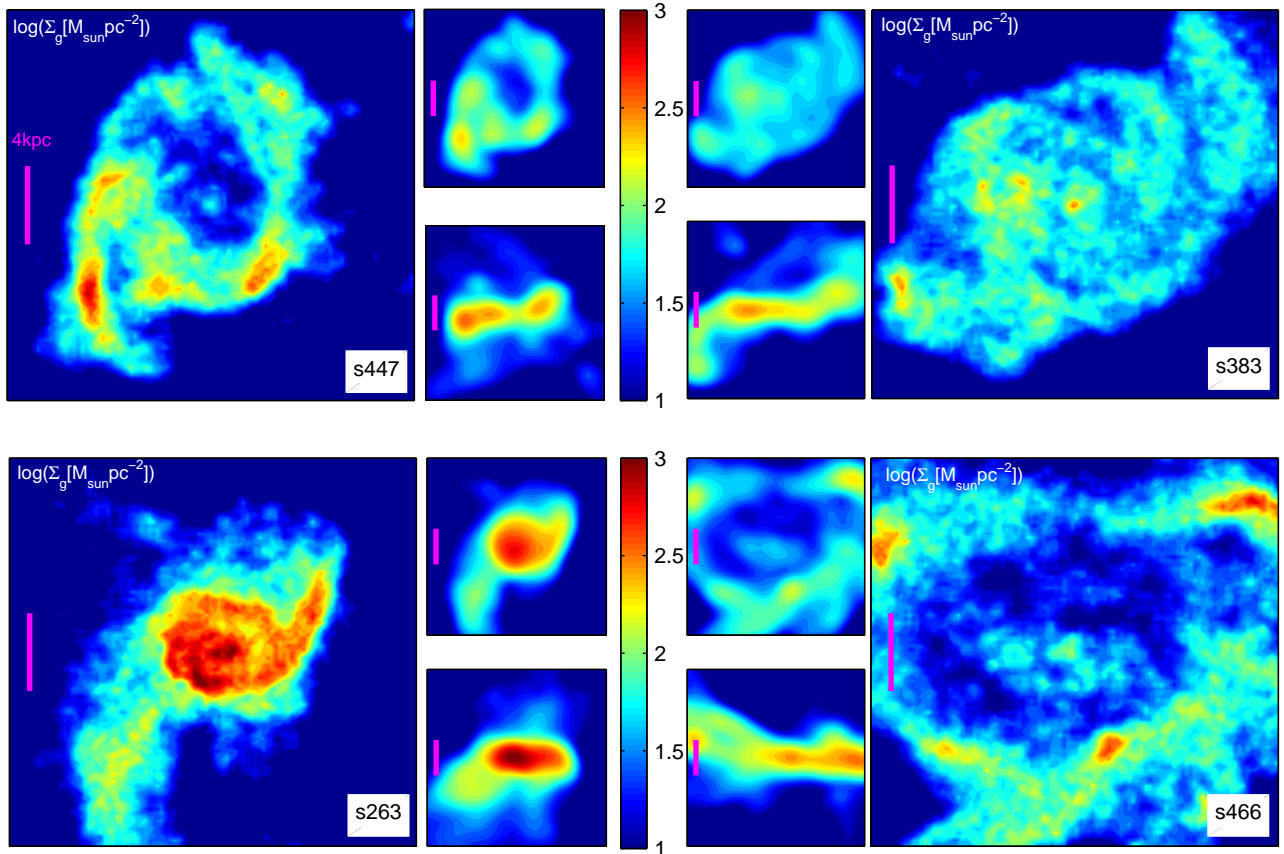


FIG. 2.— Gas surface density maps (in $M_{\odot} \text{pc}^{-2}$ on a log scale) of four simulated galaxies from our sample. The large panels are maps with resolution compared to the spatial resolution of the simulation. The small panels show the corresponding maps after they have been smoothed with two-dimensional Gaussians with $\text{FWHM}=1.5 \text{ kpc}$, in order to imitate the appearance of the galaxies under the highest available resolution of AO-assisted observations. The small panels show both face-on (*top*) and edge-on (*bottom*) views. All panels are 20 kpc on a side, and all the magenta bars are 4 kpc long. It is evident that the qualitative appearance of the simulated galaxies is similar to the clump-clusters and chain galaxies observed at $z \approx 2$ (Elmegreen & Elmegreen 2005, 2006; Förster Schreiber et al. 2011b).

4. DIRECT COMPARISON TO SINFONI OBSERVATIONS

Figure 6 shows mock SINFONI maps for $s224$ of $\text{H}\alpha$ intensity, velocity and velocity dispersion. They were obtained by converting SFR to $\text{H}\alpha$ luminosity using $L_{\text{H}\alpha}[\text{ergs}^{-1}] = 1.26 \times 10^{41} \times \text{SFR}[M_{\odot} \text{yr}^{-1}]$ (Kennicutt 1998), ‘placing’ $s224$ at $z = 2.2$, convolving it with a Gaussian to imitate a resolution of $\text{FWHM} = 0.17''$, and pasting it into a real SINFONI datacube with pixel scale $0.05''$ that was obtained from the observations of a galaxy from the SINS survey, at a redshift where no real galaxy exists. This results in realistic resolution and noise properties that correspond to a representative total integration time ($\approx 6 \text{ hours}$) for our high-resolution SINFONI data sets (Förster Schreiber et al. 2009; Genzel et al. 2011).

The clumpiness, smooth velocity field and relatively flat velocity dispersion map (outside the center), which are the characteristics of real SINS clumpy disks, are all well reproduced when ‘observing’ our simulations. The most significant difference to the non-degraded images in Figure 3 (the left and middle columns can be directly compared in Figures 6 and 3) is in the velocity dispersion map. The ‘beam smearing’ increases the apparent velocity dispersion where there are velocity gradients (this is the reason for the diagonal feature of high dispersion in the inclined image in Figure 6(c)), and the clumps are no longer seen as clear minima. As a result, the small but present velocity gradients across the clumps get

smoothed out. Thus, because of the non-virialised state of the clumps, and their being minima in velocity dispersion, they do not show strong features in observations at the currently available resolution of $\approx 1-2 \text{ kpc}$, even if their masses are dynamically significant. This prediction is consistent with the observations of Genzel et al. (2011) (but see Ceverino et al. (2011) for alternative explanations).

5. SUMMARY AND DISCUSSION

In this paper we use ‘zoom-in’ cosmological hydrodynamical simulations that include a phenomenological model for efficient star-formation feedback in the form of fast momentum-driven winds with high mass-loading factors, to investigate the formation of star-forming disk galaxies at $z \approx 2$. Our wind model reproduces observed low baryon conversion efficiencies and high gas fractions, and we also find a good kinematical and morphological agreement with observations. In addition, we present an important numerical result, namely that in the presence of such winds, the giant clumps in $z \approx 2$ disks, which form in-situ via gravitational instability, may be short-lived and unvirialised. This is because they lose mass to galactic outflows at a rate that is higher than the rate of their dynamical evolution, such that their collapse is halted in less than a disk orbital time after their formation, and before they reach virial equilibrium. We show that this scenario is plausibly consistent with most of the available observations

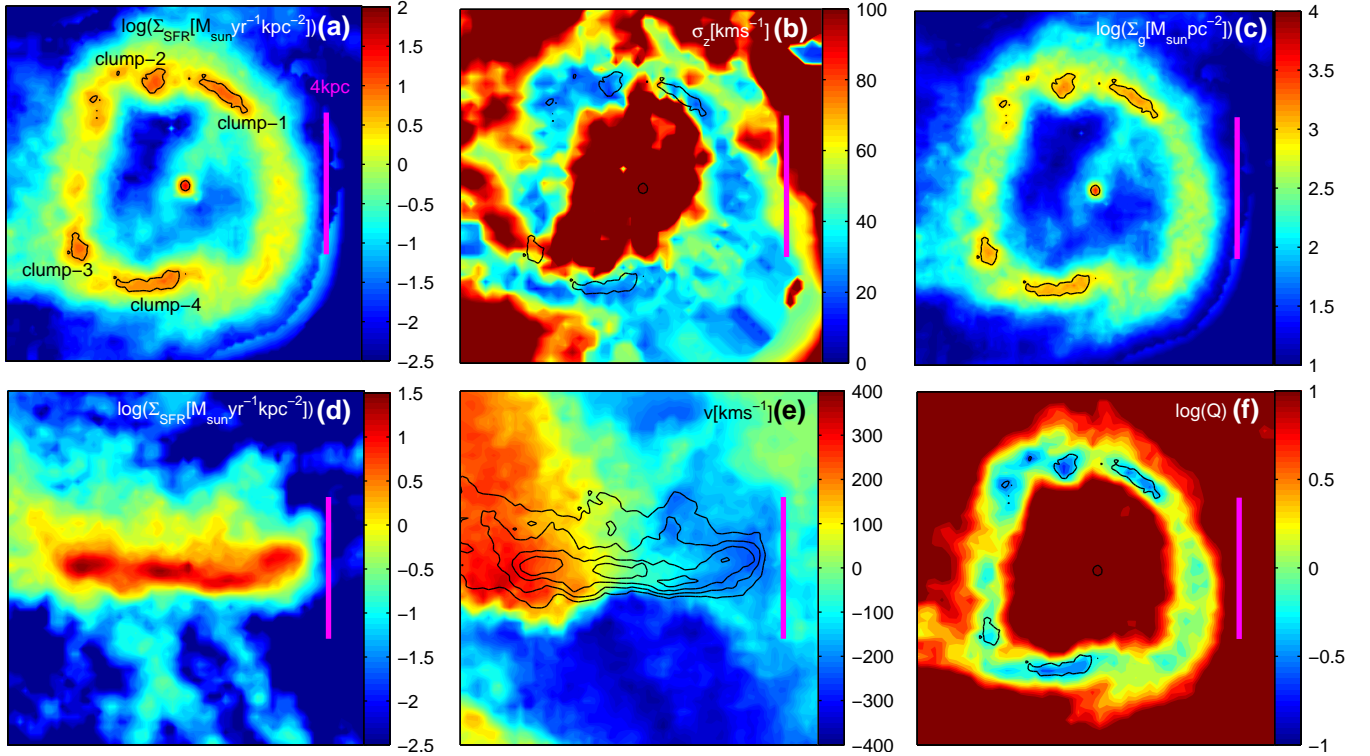


FIG. 3.— Gas properties of the central galaxy *s224* at $z = 2$. (a): face-on SFR surface density, (b): face-on line-of-sight (vertical) velocity dispersion, (c): face-on gas surface density, (d): edge-on SFR surface density, (e): edge-on line-of-sight velocity field overlotted with contours of SFR surface density and (f): $\log Q$. Each panel is 10 kpc on a side. All face-on panels are overlotted with $\Sigma_g = 1000 M_\odot \text{pc}^{-2}$ contours.

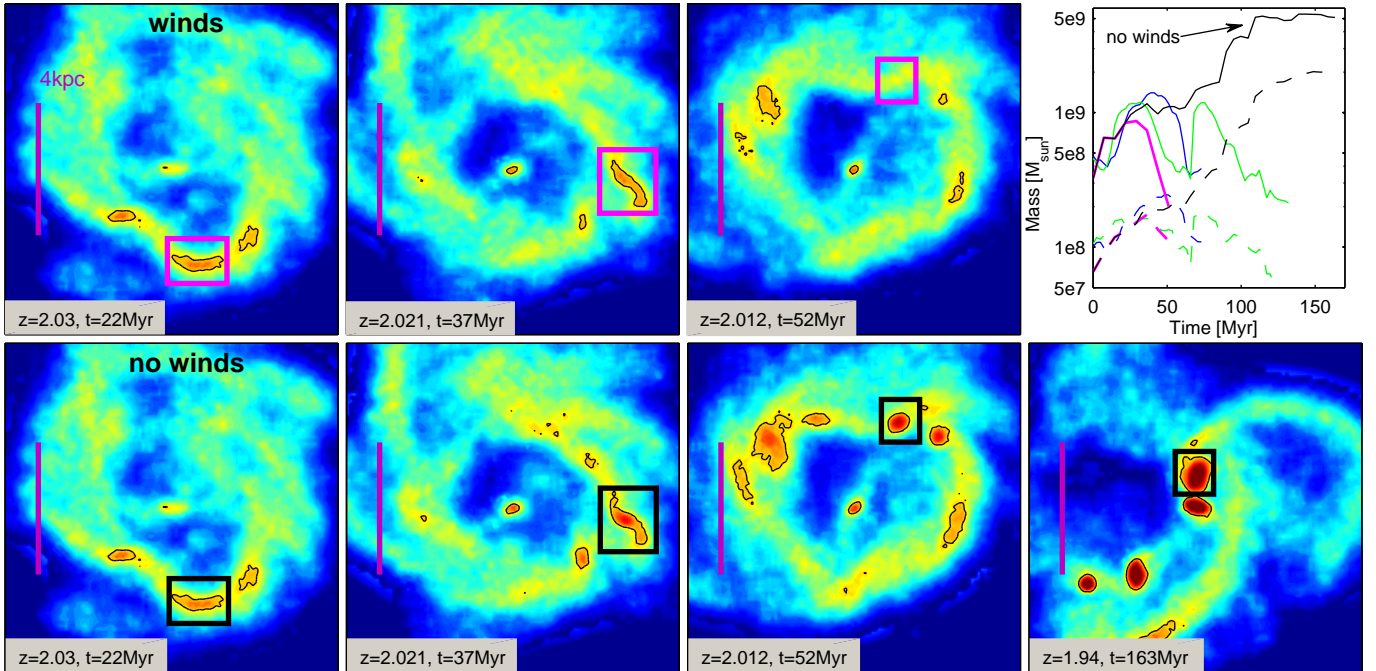


FIG. 4.— A time sequence of gas surface density maps showing the *disruption* of a clump in our model (*Top*), where $t = 0$ (not shown) is the *formation* time of the clump. To demonstrate the role of the wind, we turn it off at $z = 2.03$ ($t = 22 \text{ Myr}$) and show the alternative evolution of non-disruption, virialisation and migration (*Bottom*). The color coding is as in Figure 3(c). The upper right-most panel shows the mass of gas (*solid*) and young ($< 50 \text{ Myr}$) stars (*dashed*) for four clumps as a function of time since their formation. The magenta lines are for the clump highlighted on the *Top* and the black for the clump highlighted on the *Bottom*. The jump in mass of the green lines at $t \approx 60 \text{ Myr}$ is a result of a merger between two clumps (not shown in other panels). The typical clump lifetime in the presence of winds is $\approx 50 \text{ Myr}$, and the mass of new-formed stars is approximately 10% of the maximum clump gas mass. The mass of new-formed stars internal to the clump decreases following the decrease of the gas mass, as these stars are dispersed out of the clump when the collapse is halted by the return to $Q > 1$.

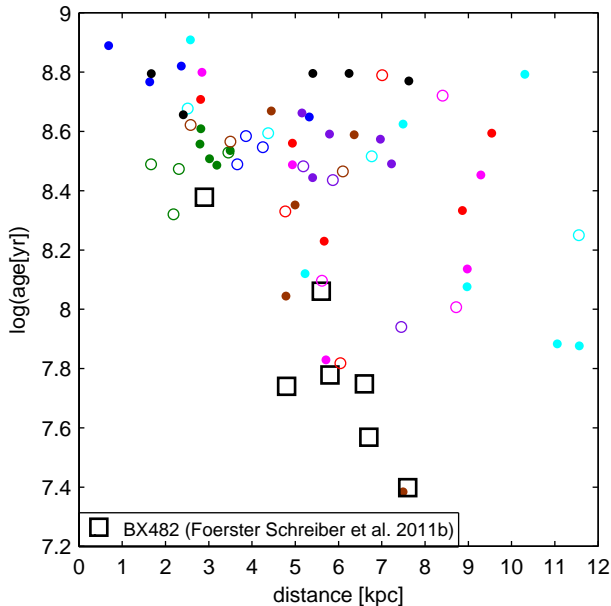


FIG. 5.— Clump stellar age (mass-weighted) versus distance from the galaxy center. Colors correspond to the different galaxies in the same way as in Figure 1, both for $z = 2$ (dots) and $z = 2.2$ (circles). More distant clumps tend to be younger, because of the dominance of ‘background’ stars in the clumps, and given the global age gradient of the galaxy. A similar relation for the clumps in the observed galaxy BX482 (‘raw’ measurements, without background subtraction) is shown as well (squares; Förster Schreiber et al. 2011b). Given that the observed ages are only relative ages, our simulations seem consistent with the observations of this galaxy. The important conclusion is that the observed trend of clump stellar age with distance (see also Genzel et al. 2008; Elmegreen et al. 2009) is not necessarily an indication for clump migration to the center of the galaxy, as has been previously considered.

of clumpy disks at $z \approx 2$: their global properties (Figure 1), their clumpiness (Figures 2 and 3), their kinematics and appearance in SINFONI observations (Figures 3 and 6), and the gradient they show between clump stellar age and clump distance from the galaxy center (Figure 5).

Our results are in contrast to previous models that do not include fast winds with high mass-loading factors. We demonstrate that if we temporarily turn off the winds, we reproduce previous results where clumps are long-lived and migrate to the galaxy centers. Therefore we are able to directly show that the winds are the critical component of our model that makes the clumps short-lived. However, if the wind is drastically reduced starting from the initial conditions of the simulations at high redshift, gas-rich unstable disks do not develop in the first place. Instead, the galaxies become gas-poor, very massive (compared to the halos inside which they form, i.e. with

very high baryon conversion efficiencies), and they develop very peaked rotation curves (see also Joung et al. 2009).

It should be stressed that our model of the winds is phenomenological, and our results are based on the working hypothesis of the existence of powerful superwinds with some given, a priori properties. Our hypothesis still awaits further verification. For example, our feedback recipe assumes that gas can be blown out of the clumps and subsequently out of the galaxy at an imposed rate proportional to the star-formation rate. It remains to be better understood how this occurs on sub-clump scales based on improved physical models (e.g. Hopkins et al. 2011). Also, the momentum we inject into the wind per unit stellar mass formed is at the high side of the theoretical expectations. While winds are observed to be ubiquitous in high-redshift galaxies, and in particular they have been recently observed from individual giant clumps, the measurements of their crucial parameters, in particular the mass-loading factors, is still very uncertain.

It has been suggested in the recent literature that the migration of giant clumps to the centers of high-redshift galaxies may serve as an avenue for the formation of galaxy bulges, in addition to the more traditional avenue of galaxy mergers (e.g. Steinmetz & Navarro 2002). The alternative scenario we present in this paper, namely that giant clumps do not migrate to their galaxy centers, does not necessarily mean that bulges do not form secularly in high-redshift galaxy disks. The instabilities and irregularities we find in our simulated disks do induce internal torques and angular momentum loss, such that inflows to smaller radii inside the disks do occur. Nevertheless, by comparing clump evolution with and without winds, we demonstrate that secular bulge growth occurs much more slowly in the case where winds disrupt clumps. We reserve detailed studies of secular bulge formation under conditions of strong feedback and giant clump destruction, as well as implications for the global cosmic rate of bulge formation, to future work.

We thank Jerry Ostriker for useful discussions. The high performance computations were performed on the HLRB-II system provided by LRZ and on the SGI-Altix 3700 Bx2 (University Observatory Munich), partly funded by the Cluster of Excellence: ‘‘Origin and Structure of the Universe’’. We thank the DFG for support via German-Israeli Project Cooperation grant STE1869/1-1.GE625/15-1. SG acknowledges the PhD fellowship of the International Max Planck Research School in Astrophysics. N.M.F.S. acknowledges support by the Minerva program of the MPG.

REFERENCES

- Agertz, O., Teyssier, R., & Moore, B. 2009, MNRAS, L263+
- Aumer, M., Burkert, A., Johansson, P. H., & Genzel, R. 2010, ApJ, 719, 1230
- Bauer, A. E., Conselice, C. J., Perez-Gonzalez, P. G., Grutzbauch, R., Bluck, A. F. L., Buitrago, F., & Mortlock, A. 2011, MNRAS, accepted (astro-ph/11062656)
- Behroozi, P. S., Conroy, C., & Wechsler, R. H. 2010, ApJ, 717, 379
- Bordoloi, R. et al. 2011, ArXiv e-prints
- Bouché, N. et al. 2007, ApJ, 671, 303
- Bournaud, F. et al. 2008, A&A, 486, 741
- Bournaud, F., Dekel, A., Teyssier, R., Cacciato, M., Daddi, E., Juneau, S., & Shankar, F. 2011, ApJ, submitted (astro-ph/11071483)
- Bournaud, F., Elmegreen, B. G., & Elmegreen, D. M. 2007, ApJ, 670, 237
- Bournaud, F., Elmegreen, B. G., & Martig, M. 2009, ApJ, 707, L1
- Burkert, A. et al. 2010, ApJ, 725, 2324
- Ceverino, D., Dekel, A., & Bournaud, F. 2010, MNRAS, 404, 2151
- Ceverino, D., Dekel, A., Mandelker, N., Bournaud, F., Burkert, A., Genzel, R., & Primack, J. 2011, MNRAS, submitted (astro-ph/11065587)
- Chabrier, G. 2003, PASP, 115, 763
- Cresci, G. et al. 2009, ApJ, 697, 115
- Daddi, E. et al. 2010, ApJ, 713, 686
- . 2007, ApJ, 670, 156
- Dalla Vecchia, C., & Schaye, J. 2008, MNRAS, 387, 1431
- Davé, R. 2008, MNRAS, 385, 147
- Davé, R. 2009, in Astronomical Society of the Pacific Conference Series, Vol. 419, Astronomical Society of the Pacific Conference Series, ed. S. Jogee, I. Marinova, L. Hao, & G. A. Blanc, 347–+
- Davé, R., Finlator, K., & Oppenheimer, B. D. 2011a, MNRAS, submitted (astro-ph/11043156)
- Davé, R., Oppenheimer, B. D., & Finlator, K. 2011b, MNRAS, 867

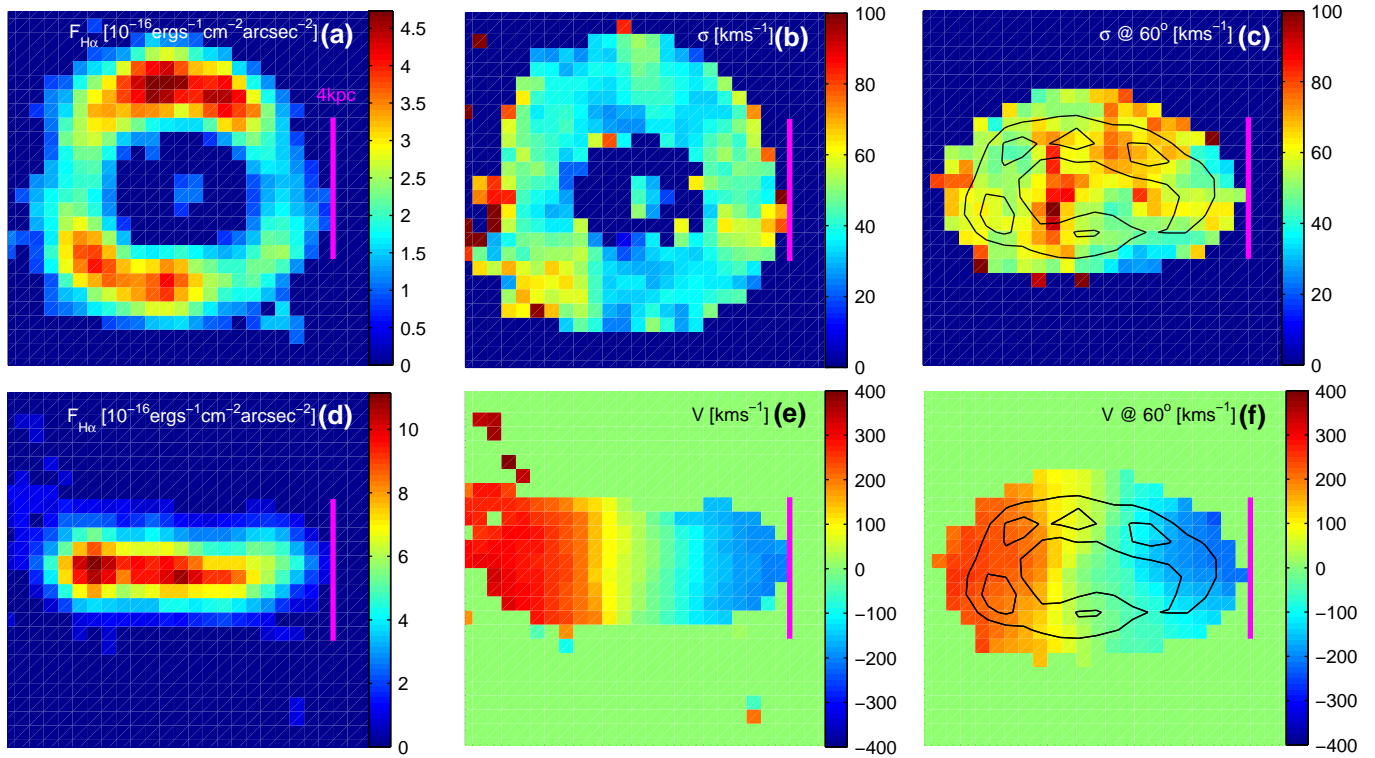


FIG. 6.— Mock $H\alpha$ line observations of the snapshot shown in Figure 3, as would be obtained with SINFONI. Face-on (a) and edge-on (d) line intensity, velocity field shown edge-on (e) and at 60° inclination (f), and velocity dispersion shown face-on (b) and at 60° inclination (c). Contours of surface density are overlotted in panels (c) and (f). See Section 4 for discussion.

- Davé, R., Oppenheimer, B. D., Katz, N., Kollmeier, J. A., & Weinberg, D. H. 2010, *MNRAS*, 408, 2051
- Dekel, A. et al. 2009a, *Nature*, 457, 451
- Dekel, A., Sari, R., & Ceverino, D. 2009b, *ApJ*, 703, 785
- Dubois, Y., & Teyssier, R. 2008, *A&A*, 477, 79
- Elmegreen, B. G., Bournaud, F., & Elmegreen, D. M. 2008, *ApJ*, 688, 67
- Elmegreen, B. G., & Elmegreen, D. M. 2005, *ApJ*, 627, 632
- . 2006, *ApJ*, 650, 644
- Elmegreen, B. G., Elmegreen, D. M., Fernandez, M. X., & Lemonias, J. J. 2009, *ApJ*, 692, 12
- Elmegreen, B. G., Elmegreen, D. M., Vollbach, D. R., Foster, E. R., & Ferguson, T. E. 2005, *ApJ*, 634, 101
- Erb, D. K., Shapley, A. E., Pettini, M., Steidel, C. C., Reddy, N. A., & Adelberger, K. L. 2006, *ApJ*, 644, 813
- Finlator, K., & Davé, R. 2008, *MNRAS*, 385, 2181
- Förster Schreiber, N. M. et al. 2009, *ApJ*, 706, 1364
- . 2006, *ApJ*, 645, 1062
- Förster Schreiber, N. M., Shapley, A. E., Erb, D. K., Genzel, R., Steidel, C. C., Bouché, N., Cresci, G., & Davies, R. 2011a, *ApJ*, 731, 65
- Förster Schreiber, N. M. et al. 2011b, *ApJ*, accepted (astro-ph/11040248)
- Fujita, A., Mac Low, M., Ferrara, A., & Meiksin, A. 2004, *ApJ*, 613, 159
- Genel, S. et al. 2008, *ApJ*, 688, 789
- Genzel, R. et al. 2008, *ApJ*, 687, 59
- . 2011, *ApJ*, 733, 101
- . 2006, *Nature*, 442, 786
- . 2010, *MNRAS*, 407, 2091
- Gnedin, N. Y., Tassis, K., & Kravtsov, A. V. 2009, *ApJ*, 697, 55
- Haardt, F., & Madau, P. 2001, in *Clusters of Galaxies and the High Redshift Universe Observed in X-rays*, ed. D. M. Neumann & J. T. V. Tran
- Hopkins, P. F., & Quataert, E. 2010, *MNRAS*, 407, 1529
- Hopkins, P. F., Quataert, E., & Murray, N. 2011, *MNRAS*, submitted (astro-ph/11014940)
- Immeli, A., Samland, M., Gerhard, O., & Westera, P. 2004a, *A&A*, 413, 547
- Immeli, A., Samland, M., Westera, P., & Gerhard, O. 2004b, *ApJ*, 611, 20
- Jones, T. A., Swinbank, A. M., Ellis, R. S., Richard, J., & Stark, D. P. 2010, *MNRAS*, 404, 1247
- Joung, M. R., Cen, R., & Bryan, G. L. 2009, *ApJ*, 692, L1
- Kennicutt, R. C. 1998, *ARA&A*, 36, 189
- Kereš, D., Katz, N., Fardal, M., Davé, R., & Weinberg, D. H. 2009, *MNRAS*, 395, 160
- Kereš, D., Katz, N., Weinberg, D. H., & Davé, R. 2005, *MNRAS*, 363, 2
- Krumholz, M. R., & Dekel, A. 2010, *MNRAS*, 406, 112
- Law, D. R., Steidel, C. C., Erb, D. K., Larkin, J. E., Pettini, M., Shapley, A. E., & Wright, S. A. 2009, *ApJ*, 697, 2057
- Leitherer, C. et al. 1999, *ApJS*, 123, 3
- Mac Low, M., & Ferrara, A. 1999, *ApJ*, 513, 142
- Martin, C. L. 2005, *ApJ*, 621, 227
- Moster, B. P., Somerville, R. S., Maulbetsch, C., van den Bosch, F. C., Macciò, A. V., Naab, T., & Oser, L. 2010, *ApJ*, 710, 903
- Murray, N., Quataert, E., & Thompson, T. A. 2005, *ApJ*, 618, 569
- . 2010, *ApJ*, 709, 191
- Oppenheimer, B. D., & Davé, R. 2006, *MNRAS*, 373, 1265
- . 2008, *MNRAS*, 387, 577
- . 2009, *MNRAS*, 395, 1875
- Oser, L., Naab, T., Ostriker, J. P., & Johansson, P. H. 2011, *ApJ*, accepted (astro-ph/11065490)
- Oser, L., Ostriker, J. P., Naab, T., Johansson, P. H., & Burkert, A. 2010, *ApJ*, 725, 2312
- Ostriker, E. C., & Shetty, R. 2011, *ApJ*, 731, 41
- Pettini, M., Steidel, C. C., Adelberger, K. L., Dickinson, M., & Giavalisco, M. 2000, *ApJ*, 528, 96
- Rodighiero, G. et al. 2010, *A&A*, 518, L25+
- Rupke, D. S., Veilleux, S., & Sanders, D. B. 2005, *ApJS*, 160, 115
- Sales, L. V., Navarro, J. F., Schaye, J., Vecchia, C. D., Springel, V., & Booth, C. M. 2010, *MNRAS*, 1326
- Schaye, J., & Dalla Vecchia, C. 2008, *MNRAS*, 383, 1210
- Schmidt, M. 1959, *ApJ*, 129, 243
- Shapiro, K. L. et al. 2008, *ApJ*, 682, 231
- . 2009, *ApJ*, 701, 955
- Springel, V. 2005, *MNRAS*, 364, 1105
- Springel, V., Di Matteo, T., & Hernquist, L. 2005, *MNRAS*, 361, 776
- Springel, V., & Hernquist, L. 2003, *MNRAS*, 339, 289
- Steidel, C. C., Erb, D. K., Shapley, A. E., Pettini, M., Reddy, N., Bogosavljević, M., Rudie, G. C., & Rakić, O. 2010, *ApJ*, 717, 289
- Steinmetz, M., & Navarro, J. F. 2002, *New Astronomy*, 7, 155
- Swinbank, A. M. et al. 2010, *Nature*, 464, 733
- Tacconi, L. J. et al. 2010, *Nature*, 463, 781
- Toomre, A. 1964, *ApJ*, 139, 1217
- van den Bergh, S., Abraham, R. G., Ellis, R. S., Tanvir, N. R., Santiago, B. X., & Glazebrook, K. G. 1996, *AJ*, 112, 359

Wake, D. A. et al. 2011, ApJ, 728, 46

Weiner, B. J. et al. 2009, ApJ, 692, 187

Zhang, D., & Thompson, T. A. 2010, ApJ, submitted (astro-ph/10054691)